

***In vitro* and *in vivo* characterization of the multiple isoforms of *Schistosoma mansoni* Hypoxanthine-guanine phosphoribosyltransferases**

Larissa Romanello¹, Ana Eliza Zeraik¹, Adriano de Freitas Fernandes¹, Juliana Roberta Torini¹, Louise E. Bird^{2,3}, Joanne E. Nettleship^{2,3}, Heather Rada^{2,3}, Yamini Reddivari^{2,3}, Ray J. Owens^{2,3}, Vitor Hugo Balasco Serrão⁴, Ricardo DeMarco¹, José Brandão-Neto⁵, Humberto D'Muniz Pereira¹.

1- Instituto de Física de São Carlos, Universidade de São Paulo, 13563-120, São Carlos, SP, Brazil. 2- OPPF-UK, Research Complex at Harwell, Rutherford Appleton Laboratory, Oxford, OX11 0FA, UK. 3-Division of Structural Biology, University of Oxford, Wellcome Trust Centre for Human Genetics, Roosevelt Drive, Headington, Oxon, OX2 7BN, 4-Laboratory Medicine and Pathobiology, University of Toronto, M5S-1A8, Toronto, ON, Canada. 5-Diamond Light Source, Harwell Science and Innovation Campus, Didcot, Oxfordshire, OX11 0DE, UK.

Corresponding author: Humberto D'Muniz Pereira – hmuniz.pereira@gmail.com/ +55 16 33739868

Abbreviations

HGPRT – hypoxanthine-guanine phosphoribosyltransferase

*Sm*HGPRT – *Schistosoma mansoni* hypoxanthine-guanine phosphoribosyltransferase

PRPP - 5-phosphorylribose 1-pyrophosphate

IMP – inosine monophosphate

GMP – guanosine monophosphate

Database

The atomic coordinates and structure factors for the *Schistosoma mansoni* hypoxanthine-guanine phosphoribosyltransferase can be found in the RCSB Protein Data Bank (<http://www.rcsb.org>) under the accession code 5IPF.

Abstract

Schistosoma mansoni, the parasite responsible for schistosomiasis, lacks the “*de novo*” purine biosynthetic pathway and depends entirely on the purine salvage pathway for the supply of purines. Numerous reports of praziquantel resistance have been described, as well as stimulated efforts to develop new drugs against schistosomiasis. Hypoxanthine-guanine phosphoribosyltransferase (HGPRT) is a key enzyme of the purine salvage pathway. Here, we describe a crystallographic structure of the *S. mansoni* HGPRT-1 (*SmHGPRT*), complexed with IMP at a resolution of 2.8Å. Four substitutions were identified in the region of the active site between *SmHGPRT*-1 and human HGPRT. We also present data from RNA-Seq and WISH, suggesting that some isoforms of HGPRT might be involved in the process related to sexual maturation and reproduction in worms; furthermore, its enzymatic assays show that the isoform *SmHGPRT*-3 does not present the same catalytic efficiency as other isoforms. Finally, although other studies have previously suggested this enzyme as a potential antischistosomal chemotherapy target, the kinetics parameters reveal the impossibility to use *SmHGPRT* as an efficient chemotherapeutic target.

Keywords: *Schistosoma mansoni*, purine salvage pathway, Hypoxanthine-guanine phosphoribosyltransferase, HGPRT.

1. Introduction

Schistosoma mansoni is a pathogenic trematode parasite that causes Schistosomiasis in humans, one of the most prevalent tropical diseases infecting approximately three hundred million people worldwide [1]. Despite its importance, this disease is neglected [2] because it is directly related to areas with precarious economic and social development, and especially a lack of appropriate sanitation [3].

The current treatment is limited to using a single drug called praziquantel. However, many reports of resistance have been described, suggesting the need for novel treatments [4, 5]. Since *Schistosoma mansoni* does not have the de novo purine nucleotide pathway, unlike its human host, it depends completely on the purine salvage pathway to supply its demands of these nucleotides [6-14]. The findings of Dovey et al. have shown that the key enzymes for purine salvage in *S. mansoni* are the phosphoribosyltransferases that catalyze the conversion of the purine bases hypoxanthine, and guanine, to their respective nucleotides IMP, and GMP, in the presence of 5-phosphorylribose 1-pyrophosphate (PRPP) [15].

Schistosomal HGPRTase has been proposed as a potential target for antischistosomal chemotherapy [8, 13] since the inhibition of this enzyme will effectively block the supply of guanine nucleotides for the parasite [15]. Small interfering RNAs (RNAis) against SmHGPRT was injected into infected mice and resulted in approximately 27% lower worm burden after a 60% reduction on the transcript levels for HGPRT [16]. Therefore, proposals suggest this represents a crucial enzyme for the survival of this pathogen, probably due to their incapability of de novo purine synthesis and the lack of interconversion between adenine and guanine nucleotides in the parasite[13].

Unlike other purine salvage pathway enzymes in *S. mansoni*, some studies have already been carried out using SmHGPRT. This protein has been previously expressed in

Escherichia coli, purified and characterized by other researchers in the past decade [15] and compared with the human HGPRT by circular dichroism [17], steady-state kinetics determined [18] and cDNA encoding analysis [19].

Despite the existence of several studies involving HGPRT, the three-dimensional structure has remained elusive for more than 20 years. In the present paper, we describe the *Sm*HGPRT crystallization and its structure determination in complex with IMP, highlighting our efforts to obtain complete structural and activity information for this important enzyme, which is crucial for the worm survival. However, while other studies have previously suggested this enzyme is a potential antischistosomal chemotherapy target [8, 13, 15, 16], the kinetics parameters described here reveal the impossibility of using *Sm*HGPRT as an efficient target.

Additionally, several studies and molecular structures of the purine salvage pathway enzymes have been released [20-28]. The description of the structure and kinetics of these enzymes permits a better understanding of the context of the metabolism of nucleotides in *S. mansoni* and represents another layer of structural and kinetic knowledge for the purine salvage pathway, which could help in the design of novel antischistosomal drugs.

2. Materials and methods

2.1. Cloning, expression and purification of Hypoxanthine-Guanine Phosphoribosyltransferase

The coding sequence for hypoxanthine-guanine phosphoribosyltransferase isoforms were obtained by searching the *S. mansoni* genome project database, HGPRTs, namely *Smp_103560.1*, *Smp_148820.1*, *Smp_168500.1* and *Smp_049850.1*, henceforth referred as *SmHGPRT-1*, -2, -3 and -4, respectively.

Primers were initially designed aiming the cDNA amplification corresponding to the complete sequence of 249 amino acids retrieved from the database. This sequence was amplified, cloned into pGEM propagation vector followed by its cloning into the expression vector pET28a(+), expressed in *Escherichia coli* BL21(λ -DE3) inserted in a 2XYT growth medium and purified through a Ni²⁺-NTA column affinity process. With the purified enzyme several crystallization tests were performed, varying the crystallization kit, enzyme concentration (5, 7, 10 mg/mL) natural ligands (IMP, GMP, PRPP, Guanine and Hypoxanthine) and temperature (4 °C, 10 °C and 18 °C). None of these trials were successful. These results led to the reanalysis of the amino acid sequence, which suggested the insertion of 18 amino acids at the beginning of the sequence. New primers were designed on the attempt of amplifying the cDNA based on the second methionine found on the sequence.

Amplified cDNA for the first three isoforms were obtained by PCR using *PhusionTM Flash High-Fidelity*. The amplification product was treated with 10 U of DpnI for 1 hour at 37 °C and purified using AMPure magnetic-beads (BeckmanCoulter).

About 3 μ L of purified amplification product and 1 μ L (~100 ng) of the appropriately linearized pOPIN vector (pOPINS3C, producing a protein in fusion with His-tag-SUMO; pOPINTRX, His-tag-thioredoxin; pOPINE, His-tag in C-terminal; pOPINM, His-tag-MBP (*maltose-binding protein*) and pOPINF, His-tag in N-terminal) derived from pTriEx2 vector that allows expression in multiple hosts, plus 6 μ L of water were mixed in the wells of an *In-Fusion*TM Dry-Down 96-well plate and incubated at 42 °C for 30 min [29].

All reactions were diluted 1:5 with T.E. Buffer (10 mM Tris pH 8.0, 1 mM EDTA) and 5 μ l used to transform 50 μ l OmniMaxII T1-phage resistant cells (Invitrogen) in 96-tube format. Transformants were selected by plating on 24-well culture plates containing 1 ml of LB Agar/well, supplemented with the carbenicillin (50 mg/ml)/0.02% w/v X-Gal and 1 mM IPTG, and incubation overnight at 37 °C, as described by Berrow *et al.* [30]. LB medium (1.2 mL) was inoculated with white colonies (two per vector) supplemented with carbenicillin (50 mg/ml) in deep wells plates, after growing 16 hours at 200 rpm, the cells were harvest by centrifugation, and bacteria pellets were used for plasmid extraction using QIAgen BioRobot 8000 and Promega Wizard prep kit. The content of each plasmid was checked by PCR using T7F and a gene-specific reverse primer. The purified plasmid was transformed into *Escherichia coli* Lemo21(DE3). Cells transformants with this plasmid were selected on LB agar plates containing carbenicillin (50 mg/ml) and chloramphenicol (35 mg/mL), 20% X-Gal and 0,5 mM IPTG.

Initial expression screening was performed using LB medium, and as result the following constructs were selected for large scale expression: HGPRT1-pOPIN-F, HGPRT2 and HGPRT3 in pOPIN-S3C expression vector.

Positive colonies were inoculated in LB medium and shaken overnight at 37 °C. Expression was performed PowerBrothTM medium supplemented with carbenicillin (50 mg/ml) and chloramphenicol (35 mg/mL), inoculated with 1:100 of overnight culture and

grown to an OD₆₀₀ of 0.6 at 37 °C. The expression was induced by the addition of 1 mM IPTG (isopropyl β-d-1-thiogalactopyranoside) and allowed to proceed overnight at 20 °C. The cells were centrifuged at 4000g for 40 min at 4 °C, suspended (3 mL: 1 g dry cellular pellet) in lysis buffer (50 mM Tris pH 7.5, 500 mM NaCl, 30 mM imidazole, 1mM MgCl₂ and 5 mM β-mercaptoethanol). The cells were lysed using a 6 min sonication and centrifuged at 13000g for 30 min at 4 °C.

The *SmHGPRTs* isoforms in the soluble fraction was purified using Talon Cobalt affinity agarose column. The column was washed with 10 column volumes using lysis buffer. The *SmHGPRTs* was eluted using elution buffer (50 mM Tris pH 7.5, 500 mM NaCl, 500 mM imidazole, 1mM MgCl₂ and 5mM β-mercaptoethanol). The purification steps were analysed by SDS-PAGE. The purified *SmHGPRT-1* was dialyzed against 50 mM Tris pH 7.5, 500 mM NaCl, 1 mM MgCl₂, 5 mM β-mercaptoethanol and 5% glycerol and concentrated to 5 mg/ml. The dialyzed *SmHGPRTs* were incubated with 5 mM IMP, GMP, PRPP, Guanine and Hypoxanthine prior crystallization screenings.

For activity assays the *SmHGPRT* samples were dialyzed into 50 mM potassium phosphate pH 7.5 supplemented with 500 mM NaCl overnight for the isothermal titration calorimetry (ITC) assays.

2.2. Crystallization and data collection

Initial crystallization trials were performed in OPPF-UK, by the sitting-drop vapor-diffusion method in Greiner 96 well plates using crystallization kits Wizard 1 and 2 (Rigaku), Morpheus, JCSG+ (Molecular Dimensions) and Index (Hampton Research). Pre-Crystallization Tests (Hampton Research) were performed to determine the optimal concentrations of protein for crystallization. Crystallization assays were achieved using the

robots Hydra and Cartesian using 100 nL drops of 5 mg/mL *Sm*HGPRT1. Plates were stored in Formulatrix at 18 °C. *Sm*HGPRT isoforms 2 and 3 failed to crystallize in all attempts.

*Sm*HGPRT1 incubated with IMP was crystallized in several conditions of the Morpheus crystallization kit (A4, A8, A9, and C9). The crystals, however, were very small, approximately 30 µm on their largest dimension. New crystallization tests were made attempting to improve the crystal and the resolution, varying the enzyme concentration (2.5; 3.5 and 5 mg/mL) and the plates incubation temperatures to (4 °C, 10 °C and 18 °C).

After screening of 200 crystals with X-rays, 21 datasets were collected on the macromolecular crystallography beamlines I24 and I04-1 at Diamond Light Source (UK) at 2.8 - 4.11 Å resolution. The best dataset (2.8 Å) contains 2,5 mg/mL enzyme incubated with 2 mM of IMP in condition A4 from Morpheus (12.5% PEG 1000, 12.5% PEG 3350, 12.5% MPD 0.03 M divalent cations, 0.1 M MES/imidazole pH 6.5) at 18 °C, in the beamline I04-1 of DLS using $\lambda = 0.9200$ Å. Data were processed automatically using Xia2 [31], XDS [32], CCP4 [32] and aimless [33] software. Table 1 shows the statistics of data collection processing and refinement.

2.3. Structure resolution and refinement

*Sm*HGPRT-1.IMP complex was solved by molecular replacement in the program Phaser [34] using human HGPRT (PDB ID 1HMP) as the search model. The model shares approximately 49% sequence identity to *Sm*HGPRT-1. Four molecules were located per asymmetric unit. Refinement was performed in Phenix [35] alternated with inspection of *Fourier* syntheses (2Fo - Fc and Fo - Fc) electron density maps and model manipulation together with ligand incorporation using Coot [36]. The parameters used for the challenging manual model building were: NCS *Ghosts Coordinates*, NCS *Maps* e NCS *Restraints*; and to

refinement: bulk solvent correction, anisotropic scaling, coordinate, ADP and occupancies refinement. MolProbity [37] was used to investigate model geometry in combination with the validation tools provided in Coot.

Crystallographic statistics are presented in Table 1 and figures were prepared with PyMOL [38]. Amino-acid sequence alignments were carried out using the program ClustalX [39]. The coordinates and structure-factor data have been deposited in the Protein Data Bank with accession codes 5IPF.

2.4. Whole mount *in situ* hybridization (WISH)

The synthesis of the digoxigenin (DIG)-labelled RNA probe was performed with the Riboprobe kit (Promega) according to the manufacturer's instructions. The template of the transcription reaction was a fragment of approximately 200 bp of HGPRT isoform 2 (Smp_148820), amplified from adult worm's cDNA using the following primers: Forward 5'-AGGCAAAGTGACTGTATAATCTTTG-3' and Reverse 5'-GAATTTAAAGCCTCCTTTCAATATACA-3' and cloned into the pGEM T-easy vector (Promega). Full-length *Sm*HGPRT isoform 1 (Smp_103560.1) in pGEM T-easy was used as a template and the resulting probe was hydrolysed to produce fragments of approximately 250 bp. WISH protocol was carried out as previously described [40, 41]. Briefly, fixed adult worms were partially digested with proteinase K, post-fixed with 4% paraformaldehyde and incubated with hybridization solution (50% formamide, 5 X SSC, 1% Tween 20 and 1 mg/mL of RNA from torula yeast) at 56 °C for 2 h. Hybridization was performed for 16 h at 56 °C in a hybridization solution containing 1 µg/mL of antisense DIG-labelled probe. Control group was incubated with sense strand riboprobe. After extensive wash steps the worms were incubated in blocking solution (100 mM maleic acid, 150 mM NaCl, pH 7.5, 0.1% Tween 20 with 10% horse serum) for 2 h prior to the addition of anti-DIG-alkaline

phosphatase-conjugated antibody (Roche), 1:2000 dilution in blocking solution (incubated overnight at 4°C). The signals were developed with NBT/BCIP (nitro-blue tetrazolium /5-bromo-4-chloro-3'-indolylphosphate) (Roche) and the worms were imaged with an Olympus BX53 microscope.

2.5. Enzymatic activity by isothermal titration calorimetry (ITC)

The enzymatic assays were conducted by isothermal titration calorimetry following the previous protocol established by Scortecci and collaborators [43] and have been commonly used for schistosomal enzymes activity detection [26-28, 44-45]. Initially, 10 μ M *Sm*HGPRT-1 and its isoforms were dialyzed in 20 mM potassium phosphate buffer at pH 7.5 and supplemented with 150 mM NaCl. Experiments to determine the enzymatic activity in the presence by the measure of apparent molar enthalpy (ΔH_{app}) were performed using guanine and hypoxanthine previously prepared in the same buffer. The enzyme was placed in the microcalorimeter cell of the isothermal titration VP-ITC (Microcal) at 25 °C and the syringe charged with 1 mM of hypoxanthine. The ΔH_{app} determination experiments were conducted using 20 μ L substrate administered in a single injection, monitoring the heat exchange for 1,200 seconds at a stirring speed of 300 rpm. After subtraction of the substrate dilution heat, the apparent molar enthalpy (ΔH_{app}) was calculated. The same procedure was repeated for the all the isoforms also using guanine as the substrate for its activity determination.

The enzymatic parameters were determined by multiple injections assays also using ITC. 5 nM *Sm*HGPRT were prepared using the same buffer as previously cited and placed into the experimental cell. The substrates were titrated in 10-25 injections (depending on the saturation and quality of the signal) of 5 μ L each stirring at 300 rpm and intervals of 180 s between the injection. All the measures were conducted at 25 °C and the collected data were analyzed by Microcal ITC-Origin software after the dilution correction and using the model

for one binding site. The same procedures were repeated to all the isoforms also to evaluate the guanine activity. All the experiments were conducted in biological triplicate to averages and standard deviation determination.

3. Results and Discussion

3.1. *S. mansoni* HGPRT isoforms have specialized roles related with the sexual biology of the parasite

Analysis of the annotated *S. mansoni* genome allows the detection of four different genes coding HGPRTs, namely Smp_103560.1, Smp_148820.1, Smp_168500.1 and Smp_049850.1, henceforth referred as *SmHGPRT*-1, -2, -3 and -4, respectively. This number of genes contrasts with humans where only a single gene coding for the HGPRT is observed. Examination of the genome sequence shows that all genes are located in a ~500kbp long portion of the chromosome 4, thus suggesting a relatively recent divergence of these genes. *SmHGPRT*-1 and *SmHGPRT*-3 are close neighbors being only separated by a ~18 kbp intergenic region and the same occur with *SmHGPRT*-2 and *SmHGPRT*-4, which are separated by a ~17 kbp intergenic region. Alignment of these sequences shows that *SmHGPRT*-4 is very similar *SmHGPRT*-2, but apparently, display a deletion in the end portion of the domain (Fig. 1). Phylogenetic analysis of HGPRTs shows that several of the duplication's events that led to the emergence of several copies of HGPRTs in *S. mansoni* appear to precede the divergence between this species and *S. japonicum*. The exception is the duplication that generated *SmHGPRT*-2 and *SmHGPRT*-4, which appear to be species specific. In contrast, *Taenia solium*, a cestode parasite, displays only two copies distantly related to the Schistosoma copies, and the two-vertebrate species analyzed have only one copy.

Previously published expression profiles of these related genes in adult worms showed significant over-expression of isoforms *SmHGPRT*-2 and -4 in males, and *SmHGPRT*-1 in females resulting from bisexual infections as compared to those from single-sex infections [46] (Supplementary Table 1). This suggests that these genes may be related to sex-specific process triggered by sexual maturation, occurring when adult parasites are in contact with members of the opposite sex.

WISH experiments using a probe for *Sm*HGPRT-2 revealed staining along the body of male and female worms (Fig. 2). In males, the staining is coincident with the gynaecophoric canal (Fig. 2 A arrow), where the female resides, possibly indicating a sexual specialization role of this enzyme.

3.2. *Sm*HGPRT-1 Structure

The *Sm*HGPRT's isoforms were cloned into a selection of pOPIN vectors [29] and after pilot expression, the pOPINF (6His-Tag in N-terminus) vector was selected. The yield was ~10 mg per liter of Power BrothTM. The protein was readily purified in a single step using Talon resin.

*Sm*HGPRT isoform 1 was selected for the crystallization trials based on the *Homo sapiens* HGPRT sequential similarity. The *Sm*HGPRT-1 in complex with IMP crystallizes in an orthorhombic system and the systematic absences indicated space group $P2_12_12_1$ with four polypeptide chains in the asymmetric unit, respectively. The crystallographic statistics and model geometry (Table 1) indicate the quality of the obtained model. IMP, a product of the catalyzed reaction, was present in the crystallization conditions; furthermore, well-defined electron density for the ligand was observed in the active site.

The refinement was completed by program Phenix and Coot for values $R_{\text{work}} = 23.17\%$ e $R_{\text{free}} = 29.0\%$. The global structure consists of α -helix and β -sheets. *Sm*HGPRT-1 chain can be divided into two domains: core and hood. The core domain is highly conserved in HGPRTs and comprises residues 41 – 173, which form four parallel β -strands (β_2 , β_3 , β_4 e β_5) and three α -helices (α_3 , α_4 e α_5) organized in doubly wound α/β -sheet [42]. This domain also comprises the loop II, which has a disordered region with no electronic density for residues 108QIGSSA122. The Domain hood is above the domain core, consisting of residues 8 – 40 and 174 – 224; it forms four small β -strands (β_1 , β_6 , β_7 e β_8) organized in two β -

330 sheets, one antiparallel and the other parallel, as well as three small α -helices ($\alpha 1$, $\alpha 2$ and
331 $\alpha 6$) and several long loops (Fig. 3).

332 The *Sm*HGPRT-1 structure crystallized as a tetramer in the asymmetric unit. The
333 oligomeric state was confirmed by gel filtration experiments (data not shown). Quantitative
334 comparison of three-dimensional structures to determine structural similarity between
335 *Sm*HGPRT-1 chains the RMSD (*Root-mean square deviation*) values are A-B = 0.304 Å, A-
336 C = 0.448 Å, A-D = 0.315 Å, B-C = 0.336 Å, B-D = 0.336 Å e C-D = 0.387 Å. The most
337 significant difference is observed in the mobile loop II region, where the A chain has a clear
338 electronic density for a greater number of residues in relation to the B, C and D chains.

339 Canyuk et al. [43] point out that enzymes that use 6-oxopurines as substrates, including
340 HGPRTs, are potential targets for the development of drugs in the treatment of diseases
341 caused by parasites. For this reason, a large number of crystallographic structures of HGPRTs
342 are reported. A comparison of the translated *Sm*HGPRT-1 peptide sequence with all HGPRTs
343 from PDB indicated ten residues (Leu74, Gly76, Leu84, Glu140, Asp141, Thr148, Lys172,
344 Gly196, Asp200 and Arg206) that are conserved among them (data not shown).

345 The quantitative comparison of three-dimensional atoms positions of the *Sm*HGPRT-1
346 structure with the human HGPRT structure resulted in an RMSD of 1.154 Å, which is
347 indicative of a high similarity between the structures. However, there are several points
348 between the structures that do not completely overlap and thus, present great differences in
349 the orientation and composition of the secondary structure. For example, β -strands are more
350 elongated in the human structure and loop II is completely ordered.

351 HGPRTs structures were previously reported as dimers and tetramers. The structure of
352 *Thermus thermophilus*, *Thermoanaerobacter tengcongensis* and *Toxoplasma gondii*, is
353 described as tetrameric [44]. Human HGPRT exists as a dimer and tetramer in solution,
354 depending on the pH and ionic strength [45] and has been crystallized as a tetramer [46]. The

Trypanosoma cruzi enzyme crystallized as a dimer [47] but was reported as a monomer in solution in the apo form and as a dimer when PRPP is bound [48]. This structure, as well as that of *Tritrichomonas foetus*, which is dimeric in the crystallographic structure are deleted in the N-terminus. In human HGPRT, this sequence was shown to be important in the formation of tetrameric interactions [46].

3.2.1. Active site

The *Sm*HGPRT-1 active site is located in the interface of the core and hood domains and comprises 4 loops: I – IV (Fig. 4), similar to that observed in other HGPRTs. The loop I corresponds to residues 73VLKGGF78 located between the β 2 strand and the α -helix 4, which are part of the $\alpha/\beta/\alpha$ motif in the core domain. The peptide bond for the residue Leu74 is in a cis configuration, as observed in other HGPRTs [47, 49-52]. Studies performed with mutants of the *Trypanosoma cruzi* HGPRT enzyme also indicated that the loop I of the active site, which participates in the dimer interface of the enzyme, has a profound influence on enzymatic efficiency [43]. The Lys75 side chain (*S. mansoni*) of the loop I from the B chain interacts with the Val103 main chain of the opposing subunit A. This hydrogen bond makes the invariant residue Arg206 oriented at the active site in the correct position for interaction with PRPP or PPI. The same conformation of these residues can be observed in the *Leishmania tarentolae*, *Toxoplasma gondii*, *Plasmodium falciparum*, *Escherichia coli*, *Trypanosoma cruzi* and human HGPRT structures [43, 51].

Loop II corresponds to residues 107 to 134 located between the β 3 and β 4 strands of the $\alpha/\beta/\alpha$ motif of the core domain. This loop was previously characterized as flexible in other HGPRT structures [46, 49, 52, 53] and it is not completely resolved in our structure due to lack of electronic density for residues 108 to 124. It was observed that the active site in these structures is open for substrate binding or release of the product and a closed

conformation should be dependent on movement of this flexible loop [46]. Subsequently, this hypothesis was confirmed in the *Trypanosoma cruzi* HGPRT structure where the two subunits differ mainly in the “flexible loop” (loop II) conformation, with one subunit open and exposed for the solvent and the other closed for the solvent [47]. In the closed conformation, interactions are observed between loop II with PRPP and with hydrated metal ions (Mg^{2+}). In the *SmHGPRT-1* structure, loop II is disordered, as observed in most open conformation structures and can be attributed to the fact that the structure contains a reaction product molecule (IMP) bound to the active site.

Loop III comprises residues 141DIIDTG146 between β 4 strand and α -helix 5, also in the core domain. In the crystallographic structure of *SmHGPRT-1* this loop is well defined. All HGPRT structures present an invariable Asp141 in loop III. Studies with mutant of this residue in *Trypanosoma cruzi* have confirmed that this residue acts in catalysis, but is not required as a general base in this position, as was previously proposed for human HGPRT [54].

Loop IV is the only one of the four loops that belongs to the hood domain; it is the largest of the four and comprises residues 190 to 211. The aromatic residue Phe193 is found in this loop that participates in the active site with π - π stacking interaction with the aromatic ring of the purine base. In several structures, this loop contains a small β -strand inside; this strand is involved in the binding of the purine base in the active site [51]. Loop-IV also has several residues at the dimeric interface in all HGPRTs deposited in the database. Loop IV is one of the loops that composes the active site. In *SmHGPRT-1*, the residue Asp207B is involved with hydrogen interactions at this interface with three water molecules and the residue Glu89A. The fact that several residues close to the active site of the loop I and loop IV participate in both dimerization and active site composition may explain the activity of the HGPRT enzyme in the dimeric and tetrameric form [43, 51].

In the *Sm*HGPRT-1 structure in complex with IMP, the phosphate of the IMP binds hydrogen with Asp144, Thr145, Gly146 and Lys147 of loop III, Thr148 of the α - helix 5 and a molecule of water. The O2 of the ribose forms two hydrogen bonds with Asp141 from loop III and two molecules of water. O3 forms a hydrogen bond with one of the water molecules that O2 bonds. The interaction of Asp141 from loop III with the ligand can be observed in the *Trypanosoma cruzi*, *Escherichia coli*, human and *Toxoplasma gondii* structures, where the side chain points towards the active site. However, the Asp141 side chain points out of the active site and does not interact with the ligand in the *Leishmania tarentolae*, *Plasmodium falciparum*, *Tritrichomonas foetus* and human structures in complex with GMP [51]. Hypoxanthine N1 forms a hydrogen bond with Val194 from loop IV and the hypoxanthine N6 with Val194 and Lys172. Thus, loop III contributes most to anchoring the IMP in the active site through hydrogen bonds. Most contacts occur between *Sm*HGPRT-1 and the IMP's phosphate group (Fig. 5). In some HGPRT structures, the presence of the magnesium ion (Mg^{2+}) in the region of the active site has been reported [49, 55-57]. Although this ion was present in the protein dialysis buffer and in the Morpheus crystallization kit, the presence of Mg^{2+} in the *Sm*HGPRT-1 active site was not observed. This absence may be the result of a lack of resolution to discern this ion in our electron map.

When overlapping the regions corresponding to the *Sm*HGPRT-1 and human active sites, a high degree of conservation around the binding and active site is observed; however, four substitutions are present: I149M, P176R, V189I and R192K (the numbering refers to the positions in *Sm*HGPRT1-Fig. 6). Three *S. mansoni* residues, namely I149, V189 and R192, superimpose well on the corresponding human residues when the two structures are compared, implying that they do not promote rearrangements in the three-dimensional structure. In contrast, the P176 residue is located in a loop region. In the human HGPRT, this loop is in a more closed conformation relative to the active site compared to *Sm*HGPRT-1

and the side chain of the residue Arg169 points into the active site, while in *Sm*HGPRT-1 the corresponding Pro176 is more distal. Among the conserved residues, differences in the side chain conformation can be seen, for example, residue Lys75 points out of the active site, while the Lys68 residue side chain of the human HGPRT points into the site. These residues compose loop I.

3.3. Comparison of isoform's enzymatic activity

For the enzyme isoform enzymatic comparison, isothermal titration calorimetry was conducted using isoforms 1, 2 and 3 purified as previously described. Initially, the kinetic determination by calorimetric assays requires the apparent enthalpy variation (ΔH_{app}) determination, where 20 μ L of hypoxanthine (1 mM) were directly injected into 10 μ M of *Sm*HGPRTs. After the curve integration, an exothermal reaction profile with an approximate ΔH_{app} of - 0.35 kcal/mol was observed after the dilution heat subtraction (Table 2) for the three isoforms. The same procedure was performed using Guanine as the substrate, revealing an enthalpy variation around - 0.16 kcal/mol.

Subsequently, the kinetics parameters were determined by multiple injections, since this enzymatic reaction presents an important enthalpy contribution, allowing the heat exchange by ITC. The hypoxanthine \rightarrow IMP conversion shows the K_M values of (47 ± 6) μ M for the *Sm*HGPRT-1 (Fig. 7, Table 2), which are similar to the values previously described for this enzyme description in the BRENDA database. However, it is important to highlight the complex variability of the kinetic parameters for this class of enzyme. The Michaelis-Menten constants can vary from low micromolar range (0.52 μ M for the *Cricetulus griseus*, Chinese hamster, HGPRT) up to 126 μ M for the human HGPRT in pH 8.6. Moreover, the schistosomal HGPRT previously described reports the two values for hypoxanthine activity (3.7 and 4.2 μ M) using radioactivity measurements at low pH [15]. Human HGPRT also

presents a huge variability of K_M values, which can reinforce the weakness of this chemotherapeutic target.

Interestingly, isoforms 2 and 3 do not present a well-defined kinetic profile, which prevented the determination of constants. This profile difference could be explained by the substrate specificity for each isoform, presenting an interestingly discrimination between hypoxanthine and guanine (Fig. 7).

Furthermore, the guanine \rightarrow GMP conversion reveals similar K_M values of (29 ± 1) μ M and (30 ± 1) μ M for the isoforms 1 and 2 (Fig. 7, Table 2). Again, it was impossible to determine the kinetic parameter for the isoform 3 using the Michaelis-Menten equation. As previously described for hypoxanthine, the reported kinetics parameters for guanine also shown a large ensemble of values. The 53 entries in the BRENDA database report K_M from 1 μ M for *Artemia* HGPRT, a small shrimp-like animal, up to 500 μ M for *Bos taurus* HGPRT. The similar K_M values for schistosomal HGPRT (2.1 and 2.7 μ M) [15] and human HGPRT (1.9 – 2.9 μ M) [63] also corroborate with the barrier to them being used as a molecular target for antischistosomal chemotherapy.

4. Conclusions

The *Sm*HGPRT structure was solved in complex with IMP in the active site. The *Sm*HGPRT displays a conserved fold and tetrameric structure when compared with orthologous enzymes. The tetrameric oligomerization state is required for enzyme activity, since residues that make up the active site are also involved in interactions in the dimeric interface, guiding the invariable residue Arg206 toward the active site. Four substitutions were identified in the region of the active site between *Sm*HGPRT and human HGPRT: Ile149Met, Pro176Arg, Val189Ile e Arg192Lys. These structures increase another layer of structural information available about the *Schistosoma mansoni* purine salvage enzymes. Although substitutions in the active site and other studies have previously suggested this enzyme is a potential antischistosomal chemotherapy target, the similar K_M values for schistosomal HGPRT and human HGPRT coupled with high variability in kinetic response in solution indicate that *Sm*HGPRT alone is unlikely to be an efficient therapeutic target.

Interestingly, the isoform 3 does not present the same catalytic efficiency as another 2 analyzed isoforms; these results may help to understand the substrates' discrimination and specificity for each isoform and the expression location as well. Additionally, two *Sm*HGPRT isoforms were found to be up-regulated in paired worms and we identified transcripts for one *Sm*HGPRT isoform in the gynaecophoric canal of male adult worms, suggesting that this enzyme might be involved in the reproduction of the parasite. It should be noted, however, that the gynaecophoric canal is also an interface with the host, and that presence of *Sm*HGPRT may reflect adaptations of the parasite metabolism to respond to specific signals or metabolic changes from the host. Considering that it has been previously described that male worm growth is sensitive to signals from the immune system [58], it is tempting to speculate if nucleotide metabolism and its enzymes could be affected by such a signal

Acknowledgments

We acknowledge the Fundação de Amparo a Pesquisa do Estado de São Paulo (FAPESP) grants 2012/05532-8 (LR) 2012/14223-9 (HMP), 2013/20715-4 (AEZ), 2012/23730-1 (VHBS) and CNPq grant 474402/2013-4,140636/2013-7, 134013/2018-8 and 232251/2014-2 for financial support, Oxford Protein Production Facility (OPPF-UK) and Diamond Light Source (DLS-UK). We acknowledge Dr. Leticia Anderson and Prof. Sergio Verjovski-Almeida for providing adult *S. mansoni* worms for the WISH experiment.

Author Contributions

LR performed amplification and cloning, protein expression, purification, crystallization, data collection, data processing, structure solution and analysis, prepared figures and manuscript. AEZ performed WISH experiments and helped prepare the manuscript. AFF performed the isoforms *SmHGPRT-2* and *SmHGPRT-3* expression and purification also the enzymatic activity assays. JRTS helped crystallization trials. LEB, JEN, HR, YR and RJO helped with cloning method suitable for high-throughput expression screening at OPPF laboratory, and preparation of the manuscript. VHBS designed the enzymatic assays, performed the data analysis and helped to write and correct the manuscript. RDM performed bioinformatic and phylogenetic analysis and helped to prepare the manuscript. JBN helped data collection and data processing. HDMP conceived and managed the project, and helped with data processing, structure solution and refinement.

References

- [1] WHO, Report on Schistosomiasis, WHO, WORLD HEALTH ORGANIZATION, <http://www.who.int/mediacentre/factsheets/fs115/en/>, 2014.
- [2] P.J. Hotez, D.H. Molyneux, A. Fenwick, E. Ottesen, S. Ehrlich Sachs, J.D. Sachs, Incorporating a rapid-impact package for neglected tropical diseases with programs for HIV/AIDS, tuberculosis, and malaria, *PLoS Med* 3(5) (2006) e102.
- [3] M.J. van der Werf, S.J. de Vlas, S. Brooker, C.W. Looman, N.J. Nagelkerke, J.D. Habbema, D. Engels, Quantification of clinical morbidity associated with schistosome infection in sub-Saharan Africa, *Acta tropica* 86(2-3) (2003) 125-39.
- [4] C.R. Caffrey, Chemotherapy of schistosomiasis: present and future, *Current opinion in chemical biology* 11(4) (2007) 433-9.
- [5] A. Fenwick, J.P. Webster, Schistosomiasis: challenges for control, treatment and drug resistance, *Curr Opin Infect Dis* 19(6) (2006) 577-82.
- [6] G.W. Crabtree, A.W. Senft, Pathways of nucleotide metabolism in schistosoma mansoni. V. Adenosine cleavage enzyme and effects of purine analogues on adenosine metabolism in vitro, *Biochem Pharmacol* 23(3) (1974) 649-60.
- [7] A.W. Senft, G.W. Crabtree, Pathways of nucleotide metabolism in Schistosoma mansoni--VII. Inhibition of adenine and guanine nucleotide synthesis by purine analogs in intact worms, *Biochem Pharmacol* 26(20) (1977) 1847-55.
- [8] A.W. Senft, G.W. Crabtree, Purine metabolism in the schistosomes: potential targets for chemotherapy, *Pharmacology & therapeutics* 20(3) (1983) 341-56.
- [9] A.W. Senft, G.W. Crabtree, K.C. Agarwal, E.M. Scholar, R.P. Agarwal, R.E. Parks, Jr., Pathways of nucleotide metabolism in Schistosoma mansoni. 3. Identification of enzymes in cell-free extracts, *Biochem Pharmacol* 22(4) (1973) 449-58.
- [10] A.W. Senft, D.G. Senft, R.P. Miech, Pathways of nucleotide metabolism in Schistosoma mansoni. II. Disposition of adenosine by whole worms, *Biochem Pharmacol* 22(4) (1973) 437-47.
- [11] R.J. Stegman, A.W. Senft, P.R. Brown, R.E. Parks, Jr., Pathways of nucleotide metabolism in Schistosoma mansoni. IV. Incorporation of adenosine analogs in vitro, *Biochem Pharmacol* 22(4) (1973) 459-68.
- [12] A.W. Senft, R.P. Miech, P.R. Brown, D.G. Senft, Purine metabolism in Schistosoma mansoni, *International journal for parasitology* 2(2) (1972) 249-60.
- [13] H.F. Dovey, J.H. McKerrow, C.C. Wang, Purine salvage in Schistosoma mansoni schistosomules, *Molecular and biochemical parasitology* 11 (1984) 157-67.
- [14] F.P. Miech, A.W. Senft, D.G. Senft, Pathways of nucleotide metabolism in Schistosoma mansoni--VI adenosine phosphorylase, *Biochem Pharmacol* 24(3) (1975) 407-11.
- [15] H.F. Dovey, J.H. McKerrow, S.M. Aldritt, C.C. Wang, Purification and characterization of hypoxanthine-guanine phosphoribosyltransferase from Schistosoma mansoni. A potential target for chemotherapy, *The Journal of biological chemistry* 261(2) (1986) 944-8.
- [16] T.C. Pereira, V.D. Pascoal, R.B. Marchesini, I.G. Maia, L.A. Magalhaes, E.M. Zanotti-Magalhaes, I. Lopes-Cendes, Schistosoma mansoni: evaluation of an RNAi-based treatment targeting HGPRTase gene, *Exp Parasitol* 118(4) (2008) 619-23.
- [17] L. Yuan, C.S. Wu, S.P. Craig, 3rd, A.F. Liu, C.C. Wang, Comparing the human and schistosomal hypoxanthine-guanine phosphoribosyltransferases by circular dichroism, *Biochimica et biophysica acta* 1162(1-2) (1993) 10-6.
- [18] L. Yuan, S.P. Craig, 3rd, J.H. McKerrow, C.C. Wang, Steady-state kinetics of the schistosomal hypoxanthine-guanine phosphoribosyltransferase, *Biochemistry* 31(3) (1992) 806-10.
- [19] S.P. Craig, 3rd, J.H. McKerrow, G.R. Newport, C.C. Wang, Analysis of cDNA encoding the hypoxanthine-guanine phosphoribosyltransferase (HGPRTase) of Schistosoma mansoni; a putative target for chemotherapy, *Nucleic acids research* 16(14B) (1988) 7087-101.
- [20] J.R. Torini, L. Romanello, F.A.H. Batista, V.H.B. Serrao, M. Faheem, A.E. Zeraik, L. Bird, J. Nettleship, Y. Reddivari, R. Owens, R. DeMarco, J.C. Borges, J. Brandao-Neto, H.D. Pereira, The

molecular structure of *Schistosoma mansoni* PNP isoform 2 provides insights into the nucleoside selectivity of PNPs, *PLoS one* 13(9) (2018) e0203532.

[21] A. Marques Ide, L. Romanello, R. DeMarco, H.D. Pereira, Structural and kinetic studies of *Schistosoma mansoni* adenylate kinases, *Molecular and biochemical parasitology* 185(2) (2012) 157-60.

[22] H.D. Pereira, G.R. Franco, A. Cleasby, R.C. Garratt, Structures for the potential drug target purine nucleoside phosphorylase from *Schistosoma mansoni* causal agent of schistosomiasis, *Journal of molecular biology* 353(3) (2005) 584-99.

[23] H.M. Pereira, V. Berdini, M.R. Ferri, A. Cleasby, R.C. Garratt, Crystal structure of *Schistosoma* purine nucleoside phosphorylase complexed with a novel monocyclic inhibitor, *Acta tropica* 114(2) (2010) 97-102.

[24] H.M. Pereira, M.M. Rezende, M.S. Castilho, G. Oliva, R.C. Garratt, Adenosine binding to low-molecular-weight purine nucleoside phosphorylase: the structural basis for recognition based on its complex with the enzyme from *Schistosoma mansoni*, *Acta crystallographica. Section D, Biological crystallography* 66(Pt 1) (2010) 73-9.

[25] L. Romanello, J.F. Bachega, A. Cassago, J. Brandao-Neto, R. DeMarco, R.C. Garratt, H.D. Pereira, Adenosine kinase from *Schistosoma mansoni*: structural basis for the differential incorporation of nucleoside analogues, *Acta crystallographica. Section D, Biological crystallography* 69(Pt 1) (2013) 126-36.

[26] L. Romanello, V.H.B. Serrao, J.R. Torini, L.E. Bird, J.E. Nettleship, H. Rada, Y. Reddivari, R.J. Owens, R. DeMarco, J. Brandao-Neto, H.D. Pereira, Structural and kinetic analysis of *Schistosoma mansoni* Adenylosuccinate Lyase (SmADSL), *Molecular and biochemical parasitology* 214 (2017) 27-35.

[27] J.R. Torini, J. Brandao-Neto, R. DeMarco, H.D. Pereira, Crystal Structure of *Schistosoma mansoni* Adenosine Phosphorylase/5'-Methylthioadenosine Phosphorylase and Its Importance on Adenosine Salvage Pathway, *PLoS neglected tropical diseases* 10(12) (2016) e0005178.

[28] A.E. Zeraik, V.H. Balasco Serrao, L. Romanello, J.R. Torini, A. Cassago, R. DeMarco, H.D. Pereira, *Schistosoma mansoni* displays an adenine phosphoribosyltransferase preferentially expressed in mature female gonads and vitelaria, *Molecular and biochemical parasitology* 214 (2017) 82-86.

[29] L.E. Bird, High throughput construction and small scale expression screening of multi-tag vectors in *Escherichia coli*, *Methods* 55(1) (2011) 29-37.

[30] N.S. Berrow, D. Alderton, S. Sainsbury, J. Nettleship, R. Assenberg, N. Rahman, D.I. Stuart, R.J. Owens, A versatile ligation-independent cloning method suitable for high-throughput expression screening applications, *Nucleic acids research* 35(6) (2007) e45.

[31] G. Winter, C.M. Lobley, S.M. Prince, Decision making in xia2, *Acta crystallographica. Section D, Biological crystallography* 69(Pt 7) (2013) 1260-73.

[32] M.D. Winn, C.C. Ballard, K.D. Cowtan, E.J. Dodson, P. Emsley, P.R. Evans, R.M. Keegan, E.B. Krissinel, A.G. Leslie, A. McCoy, S.J. McNicholas, G.N. Murshudov, N.S. Pannu, E.A. Potterton, H.R. Powell, R.J. Read, A. Vagin, K.S. Wilson, Overview of the CCP4 suite and current developments, *Acta crystallographica. Section D, Biological crystallography* 67(Pt 4) (2011) 235-42.

[33] P. Evans, Scaling and assessment of data quality, *Acta crystallographica. Section D, Biological crystallography* 62(Pt 1) (2006) 72-82.

[34] A.J. McCoy, R.W. Grosse-Kunstleve, P.D. Adams, M.D. Winn, L.C. Storoni, R.J. Read, Phaser crystallographic software, *J Appl Crystallogr* 40(Pt 4) (2007) 658-674.

[35] P.D. Adams, R.W. Grosse-Kunstleve, L.W. Hung, T.R. Ioerger, A.J. McCoy, N.W. Moriarty, R.J. Read, J.C. Sacchettini, N.K. Sauter, T.C. Terwilliger, PHENIX: building new software for automated crystallographic structure determination, *Acta crystallographica. Section D, Biological crystallography* 58(Pt 11) (2002) 1948-54.

[36] P. Emsley, K. Cowtan, Coot: model-building tools for molecular graphics, *Acta crystallographica. Section D, Biological crystallography* 60(Pt 12 Pt 1) (2004) 2126-32.

- [37] V.B. Chen, W.B. Arendall, 3rd, J.J. Headd, D.A. Keedy, R.M. Immormino, G.J. Kapral, L.W. Murray, J.S. Richardson, D.C. Richardson, MolProbity: all-atom structure validation for macromolecular crystallography, *Acta crystallographica. Section D, Biological crystallography* 66(Pt 1) (2010) 12-21.
- [38] W.L. DeLANO, The PyMOL Molecular Graphics System, 2002.
- [39] M.A. Larkin, G. Blackshields, N.P. Brown, R. Chenna, P.A. McGettigan, H. McWilliam, F. Valentin, I.M. Wallace, A. Wilm, R. Lopez, J.D. Thompson, T.J. Gibson, D.G. Higgins, Clustal W and Clustal X version 2.0, *Bioinformatics* 23(21) (2007) 2947-8.
- [40] G.P. Dillon, J.C. Illes, H.V. Isaacs, R.A. Wilson, Patterns of gene expression in schistosomes: localization by whole mount in situ hybridization, *Parasitology* 134(Pt 11) (2007) 1589-97.
- [41] A.A. Cogswell, J.J. Collins, 3rd, P.A. Newmark, D.L. Williams, Whole mount in situ hybridization methodology for *Schistosoma mansoni*, *Molecular and biochemical parasitology* 178(1-2) (2011) 46-50.
- [42] J.S. Richardson, The anatomy and taxonomy of protein structure, *Adv Protein Chem* 34 (1981) 167-339.
- [43] B. Canyuk, F.J. Medrano, M.A. Wenck, P.J. Focia, A.E. Eakin, S.P. Craig, 3rd, Interactions at the dimer interface influence the relative efficiencies for purine nucleotide synthesis and pyrophosphorolysis in a phosphoribosyltransferase, *Journal of molecular biology* 335(4) (2004) 905-21.
- [44] Q. Chen, Y. Liang, X. Su, X. Gu, X. Zheng, M. Luo, Alternative IMP binding in feedback inhibition of hypoxanthine-guanine phosphoribosyltransferase from *Thermoanaerobacter tengcongensis*, *Journal of molecular biology* 348(5) (2005) 1199-210.
- [45] G.G. Johnson, L.R. Eisenberg, B.R. Migeon, Human and mouse hypoxanthine-guanine phosphoribosyltransferase: dimers and tetramers, *Science* 203(4376) (1979) 174-6.
- [46] J.C. Eads, G. Scapin, Y. Xu, C. Grubmeyer, J.C. Sacchettini, The crystal structure of human hypoxanthine-guanine phosphoribosyltransferase with bound GMP, *Cell* 78(2) (1994) 325-34.
- [47] P.J. Focia, S.P. Craig, 3rd, A.E. Eakin, Approaching the transition state in the crystal structure of a phosphoribosyltransferase, *Biochemistry* 37(49) (1998) 17120-7.
- [48] T.E. Allen, B. Ullman, Molecular characterization and overexpression of the hypoxanthine-guanine phosphoribosyltransferase gene from *Trypanosoma cruzi*, *Molecular and biochemical parasitology* 65(2) (1994) 233-45.
- [49] P.J. Focia, S.P. Craig, 3rd, R. Nieves-Alicea, R.J. Fletterick, A.E. Eakin, A 1.4 Å crystal structure for the hypoxanthine phosphoribosyltransferase of *Trypanosoma cruzi*, *Biochemistry* 37(43) (1998) 15066-75.
- [50] L.W. Guddat, S. Vos, J.L. Martin, D.T. Keough, J. de Jersey, Crystal structures of free, IMP-, and GMP-bound *Escherichia coli* hypoxanthine phosphoribosyltransferase, *Protein science : a publication of the Protein Society* 11(7) (2002) 1626-38.
- [51] P.S. Monzani, S. Trapani, O.H. Thiemann, G. Oliva, Crystal structure of *Leishmania tarentolae* hypoxanthine-guanine phosphoribosyltransferase, *BMC Struct Biol* 7 (2007) 59.
- [52] J.R. Somoza, M.S. Chin, P.J. Focia, C.C. Wang, R.J. Fletterick, Crystal structure of the hypoxanthine-guanine-xanthine phosphoribosyltransferase from the protozoan parasite *Tritrichomonas foetus*, *Biochemistry* 35(22) (1996) 7032-40.
- [53] M.A. Schumacher, C.J. Bashor, M.H. Song, K. Otsu, S. Zhu, R.J. Parry, B. Ullman, R.G. Brennan, The structural mechanism of GTP stabilized oligomerization and catalytic activation of the *Toxoplasma gondii* uracil phosphoribosyltransferase, *Proc Natl Acad Sci U S A* 99(1) (2002) 78-83.
- [54] B. Canyuk, P.J. Focia, A.E. Eakin, The role for an invariant aspartic acid in hypoxanthine phosphoribosyltransferases is examined using saturation mutagenesis, functional analysis, and X-ray crystallography, *Biochemistry* 40(9) (2001) 2754-65.
- [55] W. Shi, C.M. Li, P.C. Tyler, R.H. Furneaux, C. Grubmeyer, V.L. Schramm, S.C. Almo, The 2.0 Å structure of human hypoxanthine-guanine phosphoribosyltransferase in complex with a transition-state analog inhibitor, *Nat Struct Biol* 6(6) (1999) 588-93.

684 [56] G.K. Balendiran, J.A. Molina, Y. Xu, J. Torres-Martinez, R. Stevens, P.J. Focia, A.E. Eakin, J.C.
685 Sacchettini, S.P. Craig, 3rd, Ternary complex structure of human HGPRTase, PRPP, Mg²⁺, and the
686 inhibitor HPP reveals the involvement of the flexible loop in substrate binding, Protein science : a
687 publication of the Protein Society 8(5) (1999) 1023-31.
688 [57] A. Heroux, E.L. White, L.J. Ross, D.W. Borhani, Crystal structures of the Toxoplasma gondii
689 hypoxanthine-guanine phosphoribosyltransferase-GMP and -IMP complexes: comparison of purine
690 binding interactions with the XMP complex, Biochemistry 38(44) (1999) 14485-94.
691 [58] D.C. Hernandez, K.C. Lim, J.H. McKerrow, S.J. Davies, Schistosoma mansoni: sex-specific
692 modulation of parasite growth by host immune signals, Exp Parasitol 106(1-2) (2004) 59-61.
693 [59] J.P. Huelsenbeck, F. Ronquist, MRBAYES: Bayesian inference of phylogenetic trees,
694 Bioinformatics 17(8) (2001) 754-5.

695 Table 1 - Statistics of data collection processing and refinement.

Data Collection	HGPRT - IMP
Space Group	$P2_12_12_1$
Cell dimensions (Å) <i>a</i> , <i>b</i> , <i>c</i> .	59.95 117.96 139.37
Angles (°)	$\alpha = \beta = \gamma = 90$
Detector	PILATUS 2M
X-ray source	DLS I04-1
Wavelength (Å)	0.9200
Resolution range (Å)	60.0 - 2.8 (2.95 - 2.8)
Redundancy	3.8 (3.8)
<i>R</i> _{pim} (%)	6.3 (54.1)
CC (1/2)	0.996 (0.605)
Completeness (%)	98.0 (99.2)
Total reflections	92655 (13365)
Unique reflections	24452 (3562)
<i>I</i> / σ (<i>I</i>)	8.9 (1.4)
Refinement parameters	
Reflections used for refinement	24416
<i>R</i> (%)	23.17
<i>R</i> _{Free} (%)	29.00
No. of protein atoms	5604
No. of ligand atoms	92
<i>B</i> (Å ²)	61.56
Coordinate Error (ML based) (Å)	0.50
Phase error (°)	30.56
All- atom Clashscore	7.09

RMSD from ideal geometry	
r.m.s. bond lengths (Å)	0.002
r.m.s. bond angles (°)	0.544
PDB ID	5IPF

Table 2. Thermodynamic and kinetic parameters for binding of *Sm*HGPRT isoforms for hypoxanthine and guanine.

<i>Sm</i>HGPRT isoform	Substrate	ΔH_{app} (cal/mol)	K_M (μM)	V_{max} (μMs⁻¹)
1	Hypoxanthine	-378.0 ± 0.9	47 ± 6	0.40 ± 0.03
	Guanine	-152.8 ± 0.3	29 ± 1	2.3 ± 0.3
2	Hypoxanthine	-368.7 ± 0.8	-	2.2 ± 0.5
	Guanine	-141.6 ± 0.5	30 ± 1	2.5 ± 0.4
3	Hypoxanthine	-344.4 ± 0.8	-	0.16 ± 0.07
	Guanine	-170.0 ± 0.4	-	-

A

```

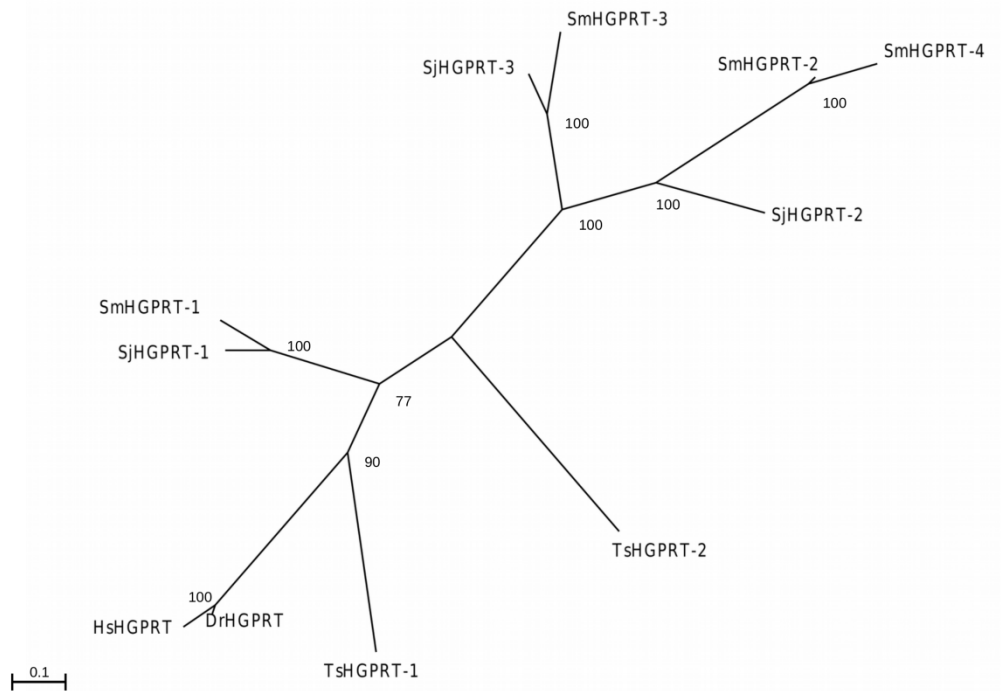
SmHGPRT-3 1 MOPS-YRKNFVVIDDFPYSEKCFNLASKYTPYESTIIPNGMIKDRLEKSIDILETFELLNATAINLLCVLKGGFKF
SmHGPRT-2 1 MASREGKSDCIIFDSDYEGYSAKMTLPPEYKHIHTILIPGGVRSRLDRMSIDILNDYKSGVKSYYIICLLKGGFKF
SmHGPRT-4 1 MASREYKNDCCIIFDSDYEGYSAKMTLPPEYKHIHTILIPGGVRSRLDRMSIDILNDYKSGVKSYYIICLLKGGFKF
SmHGPRT-1 1 MSSNMIKADCVVIEDSFGFPTFCTSPRYDECLDYVLIPNGMIKDRLEKSMNIIVDYACNATSTILCVLKGGFKF
HsHGPRT 1 WAT---RSPGVVISDDEPGYDLDFCIPNHMAEDLERVFIPAGLMDRTERLAR---DVNMEMGGHHIVALCVLKGGYKF

SmHGPRT-3 80 ASDLSEKTHNSAVTRSKSIPIFMDFIVSSITYENDIVGHEPQFHTYTNLTSEKOKVLLIVEDLLDSGTHLSRLVPYIKSFE
SmHGPRT-2 81 ASDLFKTLQKYSFTRDNYTKVSIQFVASTYVDDSVGHDTNITPCTNMEKFRKQVLLIVEDVDTGTSNLERFVRKYE
SmHGPRT-4 81 ASDLFKTLQKYSFTRRSYTKVSIQFVASTYVDDSVGHDTNITPCTNMEKFRKQVLLIVEDVDTGTSNLERFVRKYE
SmHGPRT-1 81 LAQLVDGLERTVRARGIVLPMSEFVRVKSYYNDVSIHEPILTGLGDPSEYKQVLLIVEDIDTGKTIKLISHLDLS
HsHGPRT 75 FAQLDYLKALNRNSDRSIPMTVDIFRLKSYCHDQSTGDIKVIIGDDLSTLTGKIVLLIVEDIDTGKTIKLISHLDLS

SmHGPRT-3 160 PRSVLVACLLVKKRKC-SEFQPDFVGFVPRRFEIVGYAIDYNDFFRDIPHICSDINDEAKKTFATSKSKD-- 228
SmHGPRT-2 161 PKSVYSACFSSKKQPIITFPGYKPTTYGFEVPMVEIVGYGIDYNDQFRELPMCAVNDGKREELGKG---- 227
SmHGPRT-4 161 PKSVYSAWY-----VLLMLFSLLYCHRMHNS----- 186
SmHGPRT-1 161 TSGVKVASLLVKRTSPR-NDYRPDFVGFVPRRFEIVGYALDYNDNRDLHHTGVINEVGOKKFSVPCTSKPV 231
HsHGPRT 155 PKSVKVASLLVKRTFS-VGYKPDFVGFVPRRFEIVGYALDYNEYRDLNMGVISETGKAKYKA----- 218

```

B



705

706 **Figure 1.** A) Multiple alignments of *S. mansoni* and *H. sapiens* HGPRTs. Red boxed
707 highlight amino acids from the active site that are mutated between *SmHGPRT-1* and
708 *HsHGPRT*. B) Phylogenetic tree of HGPRTs from *S. mansoni* (Sm), *S. japonicum* (Sj),
709 *Taenia solium* (Ts), *Danio rerio* (Ds) and *Homo sapiens* (Hs). The tree was constructed using
710 Bayesian inference implemented on MrBayes program [59], using default parameters. The
711 number next to each node indicates the associated posterior probability.

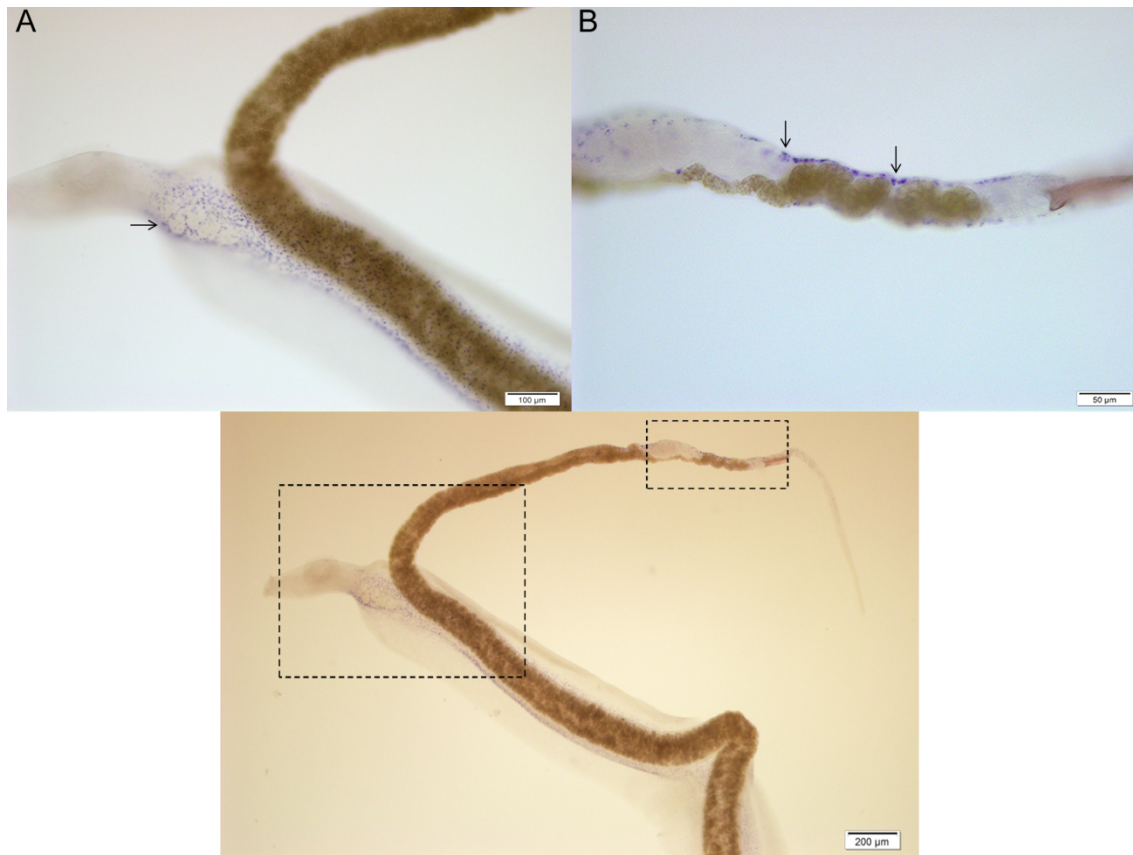


Figure 2. Localization of *SmHGPRT2* transcripts in *S. mansoni* adult worms. A) WISH experiment depicting a male worm with staining for *SmHGPRT2* transcripts in the gynaecophoric canal (arrow). B) Higher magnification views of the boxed image of a female with staining along the periphery of the body.

Domain Hood

Active Site

Loop II disordered

Domain Core

...d (red).
...ized in
...6) and
...5) and
... also
...idues

743
744
745
746
747
748
749
750
751



Active Site

Figure 4. Active site consisting of residues I, II, III, IV – red and IMP - black.

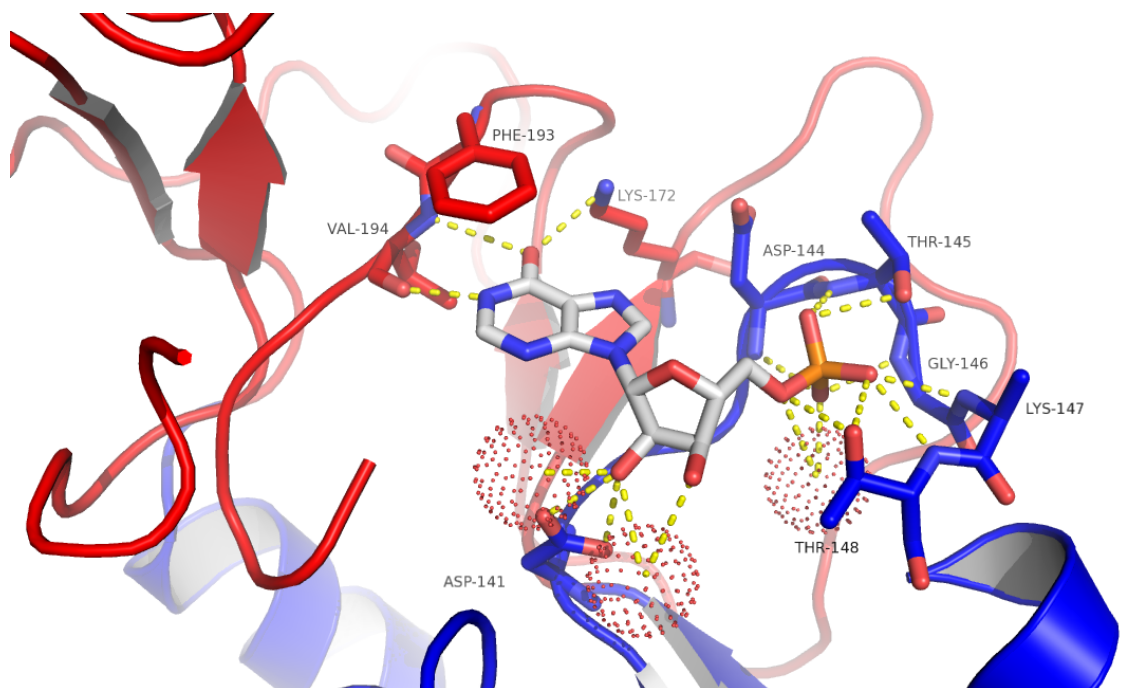


Figure 5. *SmHGPRT-1* structure in complex with IMP. Phosphate binds hydrogen with Asp144, Thr145, Gly146, and Lys147 of loop III, Thr148 of the α - helix 5 and a molecule of water. The O2 of the ribose forms two hydrogen bonds with Asp141 from loop III and two molecules of water. O3 forms a hydrogen bond with one of the water molecules that O2 bonds. Hypoxanthine N1 forms a hydrogen bond with Val194 from loop IV and the hypoxanthine N6 with Val194 and Lys172.

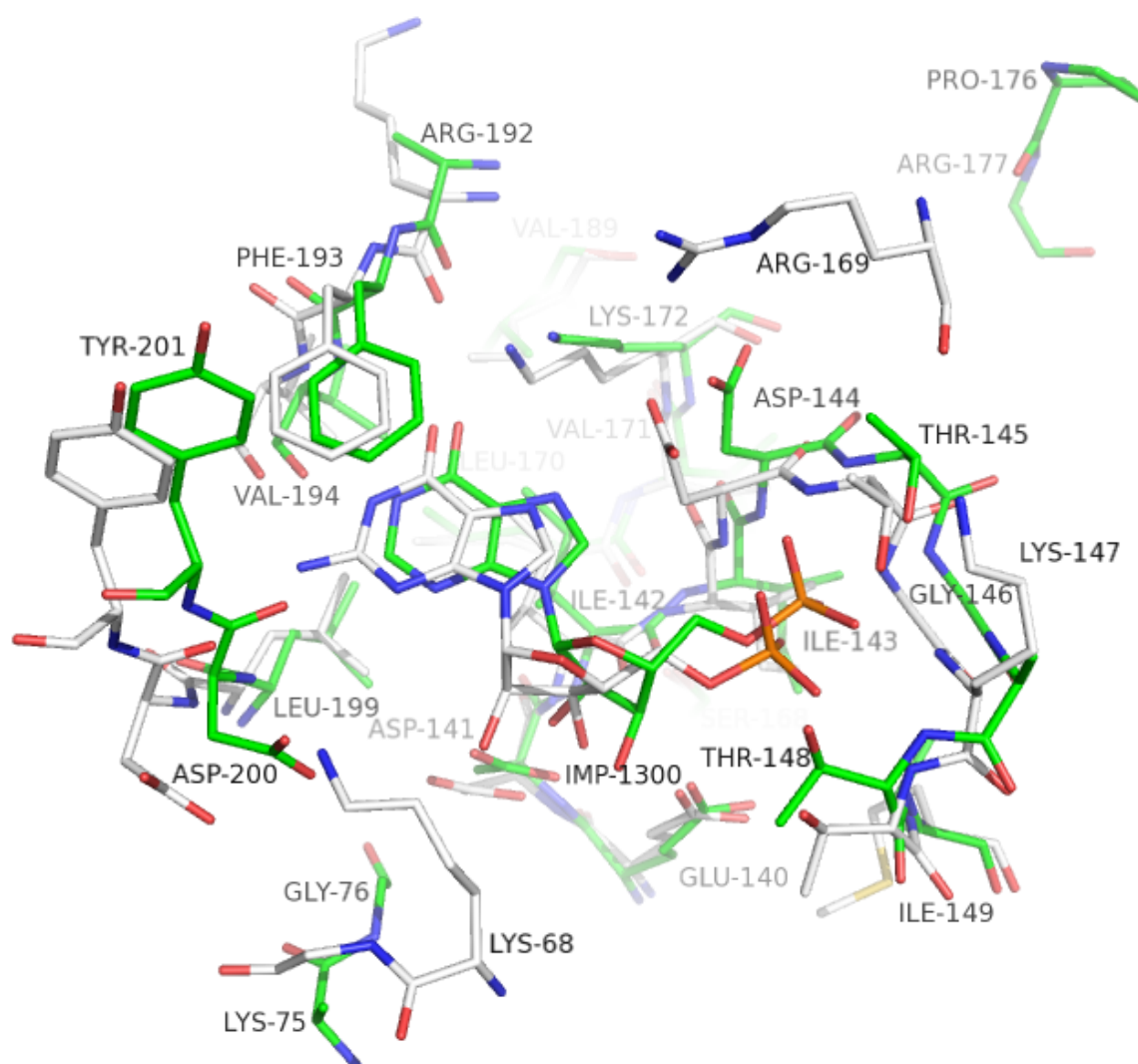
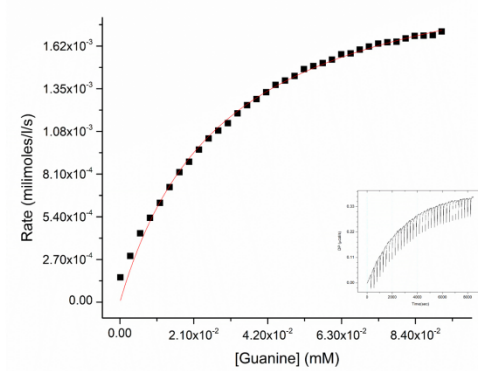
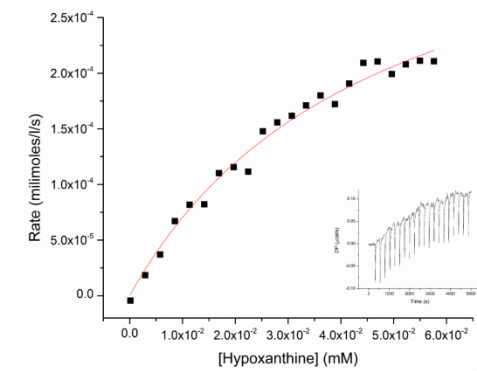
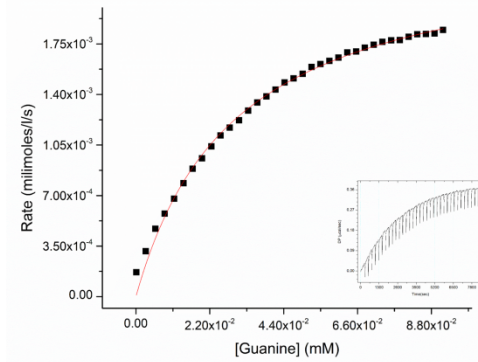
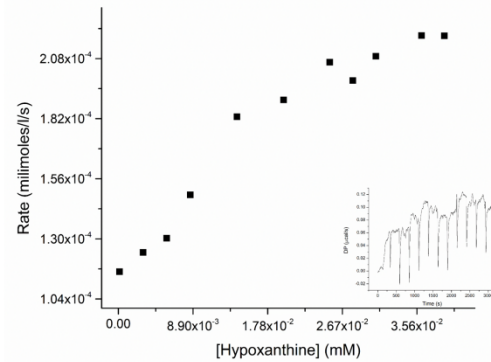


Figure 6. Superposition *SmHGPRT*-1 (green) and human *HGPRT* (white) active sites. Four substitutions are noticeable: I149M, P176R, V189I and R192K.

A



B



C

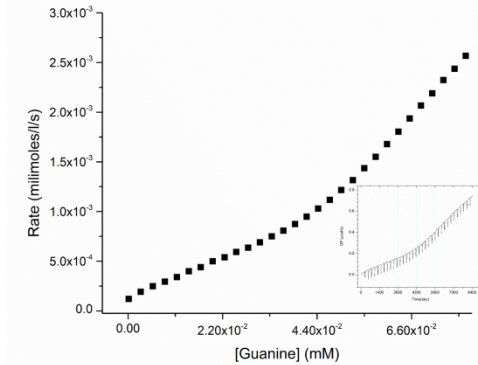
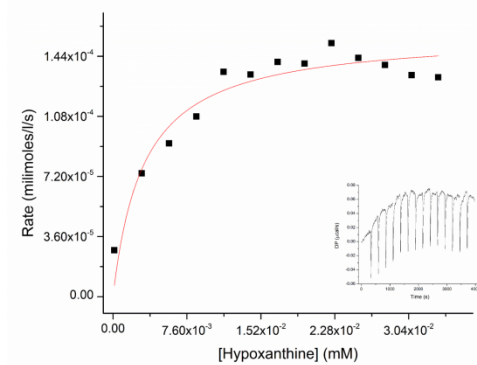


Figure 7. The enzymatic assays comparing the isoforms *Sm*HPRT-1, 2 and 3. Multiple injection by ITC showing the Michaelis-Menten kinetics profile for Guanine and Hypoxanthine as the substrates. *Inset:* the raw data for each experiment. The kinetics parameters are showed in Table 2.